Computational Mechanics 31 (2003) 38–48 © Springer-Verlag 2003
DOI 10.1007/s00466-002-0391-2

An extended finite element method with higher-order elements for curved cracks

F. L. Stazi, E. Budyn, J. Chessa, T. Belytschko

Abstract A finite element method for linear elastic fracture mechanics using enriched quadratic interpolations is presented. The quadratic finite elements are enriched with the asymptotic near tip displacement solutions and the Heaviside function so that the finite element approximation is capable of resolving the singular stress field at the crack tip as well as the jump in the displacement field across the crack face without any significant mesh refinement. The geometry of the crack is represented by a level set function which is interpolated on the same quadratic finite element discretization. Due to the higher-order approximation for the crack description we are able to represent a crack with curvature. The method is verified on several examples and comparisons are made to similar formulations using linear interpolants.

Keywords Fracture, Finite elements, Crack propagation, Extended finite element method

F. L. Satzi (✉)
Dipartimento di Ingegneria Strutturale e Geotecnica,
Università di Roma "La Sapienza"
e-mail: furio.stazi@uniroma1.it

E. Budyn
Graduate Research Assistant,
Department of Mechanical Engineering,
Northwestern University
e-mail: e-budyn@northwestern.edu

J. Chessa
Graduate Research Assistant,
Department of Mechanical Engineering,
Northwestern University
e-mail: j-chessa@northwestern.edu

T. Belytschko
Walter P. Murphy Professor of Mechanical Engineering,
Northwestern University
e-mail: tedbelytschko@northwestern.edu

Dedicated to the memory of Prof. Mike Crisfield, for his cheerfulness and cooperation as a challenge and friend over many years.

The authors are grateful for the research support by the Office of Naval Research. This work was supported in part under the auspices of the U.S. Department of Energy by the University of California, Lawrence Livermore National Laboratory under Contract No. W-74055-Eng-48. Furio Lorenzo Stazi is grateful for the research support of the Fulbright Fellowship.

1 Introduction

We describe the development of higher order elements within the setting of the eXtended Finite Element Method (X-FEM). The X-FEM is a numerical method to model arbitrary discontinuities in continuous bodies that does not require the mesh to conform to the discontinuities nor significant mesh refinement near singuliarities [2, 6, 19, 26]. In X-FEM the standard finite element approximation is enriched and the approximation space is extended by an additional family of functions. By choosing an appropriate enrichment, the extended finite element approximation space can more closely approximate the solution space for the problem considered. This type of enrichment is an application of the concept of the partition of unity [17].

For linear elastic fracture mechanics, the near tip singular stress field and the displacement discontinuity across the crack face are problematic for standard piecewise polynomial approximations. However, by adding a neartip asymptotic field and a step to the polynomial approximations we can enrich the standard FEM approximation so that good accuracy is achieved without conforming to the mesh.

This method was introduced in several papers by Belytschko and coworkers. In Belytschko and Black [2], Moës et al. [19] and Dolbow et al. [12] the crack topology was represented by an explicit discretization. Updating this explicit representation can be inconvenient when crack growth is considered. In Sukumar et al. [27] a level set representation of the topology was adopted for material interfaces. Non-planar quasi-static crack growth in three dimensions was considered in Moës et al. [20] and Gravouil et al. [16] with an orthogonal pair of level set functions to represent the crack. A PDE based method was employed to update the level sets similar to the method described in Peng et al. [22]. In all of the aforementioned papers only linear finite element approximations were used in the X-FEM approximations and in the level set interpolations. Wells et al. [34] have used the X-FEM concept in 6-node triangles in visco-plastic materials but only considered cracks that ended at an element edge.

Here we consider a technique for enriching high-order elements, and in particular quadratic finite elements. It is well known that higher-order elements provide improved accuracy for sufficiently smooth problems. Away from the crack tip this smoothness condition is satisfied in elastic problems, so improved accuracy is expected. In fact

quadratic elements are the elements of choice for most static and quasi-static elastic problems. This is due to their higher rate of convergence, their decreased susceptibility to locking, and their ability to model curved boundaries. Furthermore, a level set interpolated by quadratic shape functions is capable of describing curved cracks; level set descriptions by piecewise linear finite elements are limited to piecewise linear cracks.

An outline of this paper is as follows. In Sect. 2, the formulation of the method is presented: the governing equations and the weak forms are given. Next, in Sect. 3 the level set representation of the crack is described. In Sect. 4, the X-FEM approximation is presented and its implementation is described. The accuracy and convergence of the method in demonstrated through several example problems in Sect. 6. Conclusions are presented in Sect. 7.

2
Formulation

2.1
Governing equations

Although many of the techniques presented here are applicable to nonlinear, large deformation problems, we present them in the context of linear elasticity. Let Ω be a regular region bounded by a smooth curve Γ. The boundary of the body Γ is the union of Γ_t and Γ_u. Essential boundary conditions are imposed on Γ_u while traction boundary conditions are imposed on Γ_t. Let $\mathbf{u}$ be the displacement and ε the strain, given by:

$$\varepsilon = \nabla_s \mathbf{u} \tag{1}$$

where ∇_s indicates the symmetric part of the gradient.

If we assume that the faces of the crack Γ_{cr} are traction free, the strong form of the initial boundary value problem has the following form

$$\nabla \cdot \sigma + \mathbf{b} = 0 \quad \text{in} \quad \Omega \tag{2}$$

$$\mathbf{u} = \bar{\mathbf{u}} \quad \text{on} \quad \Gamma_u \tag{3}$$

$$\sigma \cdot \mathbf{n} = \bar{\mathbf{t}} \quad \text{on} \quad \Gamma_u \tag{4}$$

$$\sigma \cdot \mathbf{n} = 0 \quad \text{on} \quad \Gamma_{cr} \tag{5}$$

where σ is the Cauchy stress tensor, $\mathbf{b}$ the body force per unit volume, $\mathbf{n}$ the outward unit normal to Γ, $\bar{\mathbf{u}}$ the prescribed displacement and $\bar{\mathbf{t}}$ the prescribed traction. The mechanical behavior of the bodies is governed by a linear elastic constitutive law:

$$\sigma = \mathbf{C} : \varepsilon \tag{6}$$

where C is the elasticity tensor.

2.2
Weak form

We require that the trial functions $\mathbf{u}$ satisfy all displacement boundary conditions and have the usual smoothness properties so that $\mathbf{u}$ is continuous (C^0) in Ω.

$$\mathbf{u} \in \mathcal{U}, \ \mathcal{U} = \{\mathbf{u} | \mathbf{u} \in C^0 \text{ except on } \Gamma_{cr}, \mathbf{u} = \bar{\mathbf{u}} \quad \text{on } \Gamma_u\} \tag{7}$$

The test functions $\delta\mathbf{v}$ are defined by:

$$\delta\mathbf{v} \in \mathcal{U}_0,$$

$$\mathcal{U}_0 = \{\delta\mathbf{v} | \delta\mathbf{v} \in C^0 \text{ except on } \Gamma_{cr}, \delta\mathbf{v} = 0 \quad \text{on } \Gamma_u\} \tag{8}$$

The weak form of the equilibrium equation and traction boundary conditions is: find $\mathbf{u} \in \mathcal{U}$ such that

$$\int_\Omega \sigma(\mathbf{u}) : \varepsilon(\delta\mathbf{v}) d\Omega = \int_\Omega \mathbf{b} \cdot \delta\mathbf{v} \, d\Omega + \int_{\Gamma_t} \bar{\mathbf{t}} \cdot \delta\mathbf{v} \, d\Gamma \quad \forall \delta\mathbf{v} \in \mathcal{U}_0 \tag{9}$$

Recalling the linear elastic constitutive law (6) and the strain definition (1), the following weak form of the problem can be obtained: find $\mathbf{u} \in \mathcal{U}$ such that

$$\int_\Omega \varepsilon(\mathbf{u}) : \mathbf{C} : \varepsilon(\mathbf{v}) d\Omega = \int_\Omega \mathbf{b} \cdot \mathbf{v} \, d\Omega + \int_{\Gamma_t} \bar{\mathbf{t}} \cdot \mathbf{v} \, d\Gamma \quad \forall \mathbf{v} \in \mathcal{U}_0 \tag{10}$$

In Belytschko and Black [2] it is shown that the above weak form is equivalent to the strong form (2–5).

3
Geometric description of crack

It is convenient, but not essential, to represent the crack by a signed distance function $f(\mathbf{x})$, often called a level set. In this format the crack is given by the zero isobar of the function $f(\mathbf{x})$, i.e. by:

$$f(\mathbf{x}) = 0 \tag{11}$$

The signed distance function $f(\mathbf{x})$ is defined by:

$$f(\mathbf{x}) = \text{sign}[\mathbf{n} \cdot (\mathbf{x} - \bar{\mathbf{x}})] \min_{\bar{\mathbf{x}} \in \Gamma_{cr}} \|\mathbf{x} - \bar{\mathbf{x}}\| \tag{12}$$

We only define $f(\mathbf{x})$ in a subdomain around the crack as shown in Fig. 1.

In addition we define the functions $g_I(\mathbf{x})$, which locate the crack tips (I runs over the number of crack tips). The function $g_I(\mathbf{x})$ is given by:

$$g_I(\mathbf{x}) = \|\mathbf{x} - \mathbf{x}_I^{\text{tip}}\| \tag{13}$$

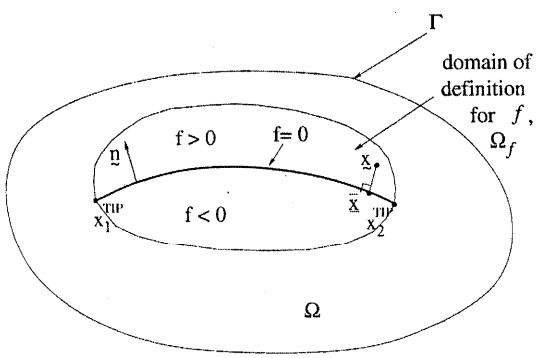


Fig. 1. Definition of signed distance function $f(\mathbf{x})$ and its representation of the crack; $\boldsymbol{n}$ is the normal to the crack over Γ_{cr}

Each of the $g_I(\mathbf{x})$ functions defines a set of circles around the crack tip as shown in Fig. 2. From any point $\tilde{\mathbf{x}}$, the location of the tip can be found by determining the intersection of $f = 0$ and the circle defined by $\|\mathbf{x} - \tilde{\mathbf{x}}\| = g_I(\tilde{\mathbf{x}})$.

The above differs somewhat from Stolarska et al. [23] and Gravouil et al. [16, 20], who used a pair of orthogonal level sets to define the crack geometry. The approach is similar to that of Ventura et al. [33, 32]. The advantage of this approach is that the crack geometry can be updated by geometric equations, thus avoiding the need to solve the hyperbolic conservation equations to update the level sets.

4
Extended finite element approximation

4.1
Description of crack geometry

In the present Section we describe briefly the finite element enrichment scheme and its implementation. The displacements are approximated by six-node triangular elements with quadratic displacements and linear strain fields. The signed distance function $f(\mathbf{x})$ is approximated by the same shape functions as the displacement:

$$f(\xi) = \sum_{I=1}^{6} f_I N_I(\xi) \tag{14}$$

where f_I are the nodal values of $f(\mathbf{x})$ and $N_I(\xi)$ are the quadratic shape functions in terms of the element parent coordinates. The approximate crack position is then given by:

$$\Gamma_{cr} = \{\mathbf{x} | f(\mathbf{x}) = 0, \quad \mathbf{x} \in \Omega_f\} \tag{15}$$

which is quadratic within each element and a piecewise continuously differentiable function. We do not define $f(\mathbf{x})$ outside Ω_f. Note that in general, slight kinks will occur at the intersection of the crack with the element edges as shown in Fig. 4. The $g_I(\mathbf{x})$ functions are not approximated. Instead in two dimensional implementations, we store the locations of the crack tips and compute the funtion by Eq. (13) as needed.

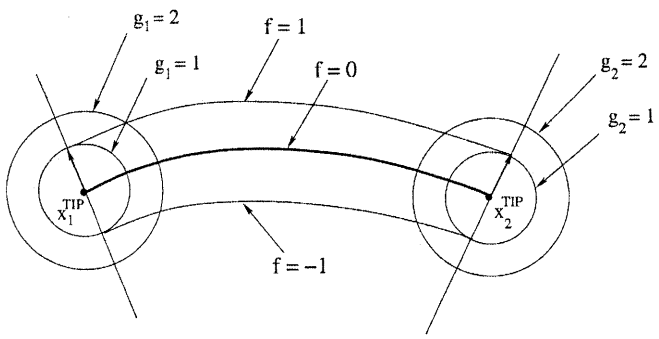


Fig. 2. Definition of tip distance function $g_I(\mathbf{x})$ of crack tip I

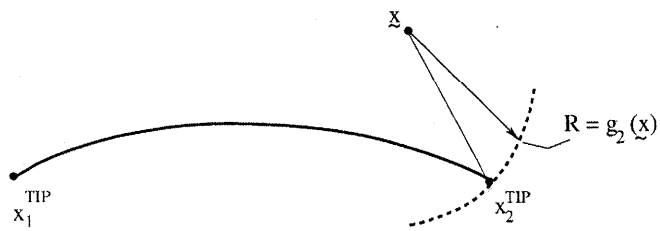


Fig. 3. Determination of crack tip location from a point x

4.2
Enriched approximation

Previously, piecewise linear finite element approximations were used in X-FEM approximation. We deviate from this trend and consider piecewise quadratic finite elements as the basis for our FEM approximation of the displacements because the quadratic elements should yield a higher accuracy than linear elements and are also capable of representing curved cracks.

In developing the enriched finite element approximation to the motion (16), it is necessary to distinguish elements in the vicinity of the crack tip, Ω^{TIP}, from elements that enclose the remainder of the crack, Ω^{cr}. The possible subdivisions are illustrated in Fig. 5a and b. The assignment of Ω^{TIP} is not unique, one can either choose only the elements in which the crack tip occurs, as shown in Fig. 5a, or a cluster of elements around the tip as shown in

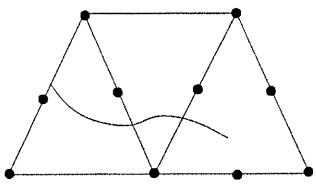


Fig. 4. Crack path as approximated by 6-node shape functions

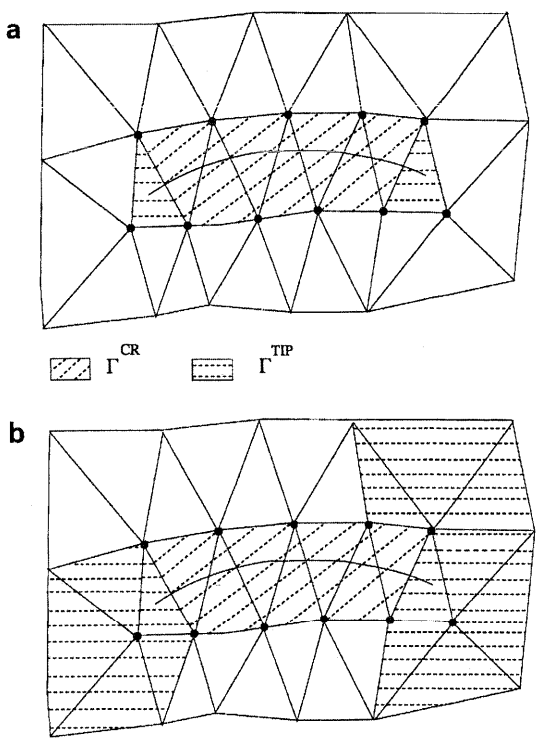


Fig. 5. The classification of elements that are modified by the crack: two possible subdivisions into Ω^{cr} and Ω^{TIP} are shown

Fig. 5b. Based on this classification, we now define three node sets which govern the enrichment:

$\mathcal{N}$ = the set of all nodes in the discretization;

$\mathcal{N}^{\text{TIP}}$ = the set of nodes that are connected to elements in Ω^{TIP};

$\mathcal{N}^{\text{cr}}$ = the set of nodes that are connected to elements in Ω^{cr} but not Ω^{TIP} .

We enrich the standard finite element approximation with the Westergaard crack tip solution at the nodes in $\mathcal{N}^{\text{TIP}}$ and enrich nodes in $\mathcal{N}^{\text{cr}}$ with the modified Heaviside function, Belytschko and Black [2] and Moës et al. [19]. The extended finite element approximation can then be written as follows:

$$\mathbf{u}^{\text{h}}(\mathbf{x}) = \sum_{I\in\mathcal{N}} N_I(\mathbf{x})\mathbf{u}_I + \sum_{I\in\mathcal{N}^{\text{cr}}} \tilde{N}_I(\mathbf{x})(H(f^{\text{h}}(\mathbf{x})) - H(f_I))\mathbf{a}_I + \sum_{I\in\mathcal{N}^{\text{TIP}}} \tilde{N}_I(\mathbf{x}) \sum_{k=1}^{4} (F^{\text{k}}(r,\theta) - F^{\text{k}}(x_I))\mathbf{b}_I^{\text{k}} \tag{16}$$

where $H(f(\mathbf{x}))$ is a modified Heaviside step function given by:

$$H(y) = \begin{cases} -1 & \text{if } y < 0 \\ +1 & \text{if } y > 0 \end{cases} \tag{17}$$

The Heaviside function has been modified to be symmetric about the crack. The shape functions $N_I(\mathbf{x})$ are quadratic whereas $\tilde{N}_I(\mathbf{x})$ are linear finite element shape functions that construct the partition of unity and the blending; see Chessa et al. [9] for an investigation of the important role of the blending. The column matrices $\mathbf{u}_I$ are the standard nodal displacements and $\mathbf{a}_I$ and $\mathbf{b}_I^l$ are additional parameters. $F^l(r,\theta)$ is the basis for the Westergaard field for the crack tip, which are defined in Fleming et al. [13]:

$$F^1(r,\theta) = \sqrt{r}\sin\tfrac{\theta}{2} \tag{18}$$

$$F^2(r,\theta) = \sqrt{r}\cos\tfrac{\theta}{2} \tag{19}$$

$$F^3(r,\theta) = \sqrt{r}\sin\tfrac{\theta}{2}\sin\theta \tag{20}$$

$$F^4(r,\theta) = \sqrt{r}\cos\tfrac{\theta}{2}\sin\theta \tag{21}$$

where $r = \|x - x^{\text{TIP}}\| = g(\mathbf{x})$.

To take into account any curvature of the crack, we use two definitions of θ. Let $\mathbf{t}$ be a vector tangent to the crack pointing to the interior of the crack. Note that f is not defined beyond the crack tips, i.e. for any point for which $\nabla\mathbf{g}\cdot\mathbf{t} < 0$. So in the vicinity of the crack tip, θ must be carefully defined. We define θ as follows: at a point $\mathbf{x}$, if $\mathbf{t}\cdot\nabla\mathbf{g} \le 0$ we use the regular polar angle from $-\mathbf{t}$. If $\mathbf{t}\cdot\nabla\mathbf{g} > 0$, θ is computed by:

$$\arctan(\theta) = \frac{-f}{\sqrt{g^2 - f^2}} \tag{22}$$

The minus sign in the above in the arctan argument is needed to reconcile this definition with the regular polar coordinates. One must be careful with the sign of f, which has to be reversed at the second tip of the crack to be consistent with the local polar orientation.

The function in (18) is discontinuous across the crack face, while the other three functions are continuous. So F^1 represents the discontinuity near the tip, while the other three functions span the Westergaard solution near the crack tip.

By substituting the displacement approximation (16) into the strain definition (23) we arrive at the following expression for the strain:

$$\varepsilon^{\text{h}} = \bar{\mathbf{B}}\bar{\mathbf{u}} = [\mathbf{B}_I^{\text{u}} \quad \mathbf{B}_J^{\text{a}} \quad \mathbf{B}_K^{b1} \quad \mathbf{B}_K^{b2} \quad \mathbf{B}_K^{b3} \quad \mathbf{B}_K^{b4}] \times \begin{bmatrix} \mathbf{u}_I \\ \mathbf{a}_J \\ \mathbf{b}_K^1 \\ \mathbf{b}_K^2 \\ \mathbf{b}_K^3 \\ \mathbf{b}_K^4 \end{bmatrix}, \quad \text{with} \quad \begin{matrix} I = 1\ldots\mathcal{N} \\ J = 1\ldots\mathcal{N}^{\text{cr}} \\ K = 1\ldots\mathcal{N}^{\text{TIP}} \end{matrix} \tag{23}$$

where $\bar{\mathbf{B}}$ is a strain displacement matrix. The matrix $\bar{\mathbf{B}}$ has the following forms:

$$\mathbf{B}_I^{\text{u}} = \begin{bmatrix} N_{I,x} & 0 \\ 0 & N_{I,y} \\ N_{I,y} & N_{I,x} \end{bmatrix} \tag{24}$$

$$\mathbf{B}_J^{\text{a}} = \begin{bmatrix} (\tilde{N}_J(H - H(\mathbf{x}_J)))_{,x} & 0 \\ 0 & (\tilde{N}_J(H - H(\mathbf{x}_J)))_{,y} \\ (\tilde{N}_J(H - H(\mathbf{x}_J)))_{,y} & (\tilde{N}_J(H - H(\mathbf{x}_J)))_{,x} \end{bmatrix} \tag{25}$$

$$\mathbf{B}_K^{\text{bl}}\big|_{l=1,2,3,4} = \begin{bmatrix} (\tilde{N}_K(F_K^l - F_K^l(\mathbf{x}_K)))_{,x} & 0 \\ 0 & (\tilde{N}_K(F_K^l - F_K^l(\mathbf{x}_K)))_{,y} \\ (\tilde{N}_K(F_K^l - F_K^l(\mathbf{x}_K)))_{,y} & (\tilde{N}_K(K_K^l - F_K^l(\mathbf{x}_K)))_{,x} \end{bmatrix} \tag{26}$$

Substituting the displacement (16) and the strain approximation (23) into the weak form (9), the standard discrete system of equations is obtained:

$$\mathbf{K}\mathbf{d} = \mathbf{f}^{\text{ext}} \tag{27}$$

where $\mathbf{f}^{\text{ext}}$ is the vector of external nodal forces and $\mathbf{K}$ the stiffness matrix:

$$\mathbf{K} = \int_{\Omega^{\text{h}}} \bar{\mathbf{B}}^{\text{T}}\mathbf{C}\bar{\mathbf{B}}\,\mathrm{d}\Omega \tag{28}$$

The expression of the external forces vector $\mathbf{f}^{\text{ext}}$ is:

$$\mathbf{f}_I^{\text{ext}} = \{\mathbf{f}_I^u; \mathbf{f}_J^a; \mathbf{f}_K^{b1}; \mathbf{f}_K^{b2}; \mathbf{f}_K^{b3}; \mathbf{f}_K^{b4}\} \tag{29}$$

$$\mathbf{f}_I^u = \int_{\Gamma_t} N_I\bar{\mathbf{t}}\,\mathrm{d}\Gamma + \int_{\Omega} N_I\mathbf{b}\,\mathrm{d}\Omega \tag{30}$$

$$\mathbf{f}_J^a = \int_{\Gamma_t} \tilde{N}_J(H - H(\mathbf{x}_J))\bar{\mathbf{t}}\,\mathrm{d}\Gamma + \int_{\Omega} \tilde{N}_J(H - H(\mathbf{x}_J))\mathbf{b}\,\mathrm{d}\Omega \tag{31}$$

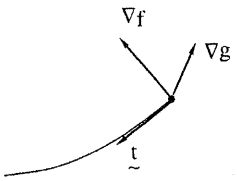


Fig. 6. Orientation at the crack tip to define the interior of the crack and the domain beyond the crack

$$\mathbf{f}_K^{\text{bl}}\big|_{l=1,2,3,4} = \int_{\Gamma_t} \tilde{N}_K(F^l - F^l(\mathbf{x}_K))\bar{\mathbf{t}}\,\mathrm{d}\Gamma + \int_{\Omega} \tilde{N}_K(F^l - F^l(\mathbf{x}_K))\mathbf{b}\,\mathrm{d}\Omega \qquad (32)$$

As with standard finite element methods, the essential boundary conditions are enforced directly on **d** which include the additional enriched degrees of freedom.

4.3 Element integration

The integration of the stiffness matrix (28) and nodal forces (29–32) in the elements with enrichments requires subelements obtained by triangular partitioning. For elements cut by a crack, the partitioning of the element is shown in Fig. 7. Three triangles are created. In each of these elements, 13 point Gauss quadrature is used.

The elements containing the crack tips are partitioned as described in Fig. 8. Four triangles are created with 13 point Gauss quadrature. The increase in computational cost is not significant.

5 Computation of the *J*-integral and Interaction-integral

The stress intensity factors were obtained by the *J*-integral and the *I*-integral. We choose a domain integral over a set of elements within a circular neighborhood about the crack tip with a radius twice the size of an average element.

The domain integral expression for the *J*-integral is:

$$J_k = \int_{\Omega} \sigma_{ij} u_{i,k} q_{k,j}\,\mathrm{d}\Omega - \frac{1}{2}\int_{\Omega} \sigma_{ij} u_{i,j} \delta_{kj} q_{k,j}\,\mathrm{d}\Omega \qquad (33)$$

In our calculation J_1 with the x_1-axis parallel to the crack face, was computed. In the above q equals 1 inside the

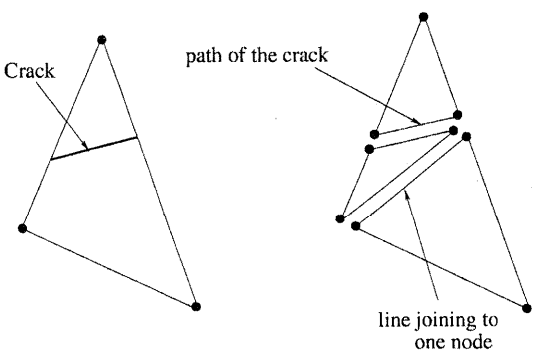


Fig. 7. Delaunay partitioning of elements cut by a crack

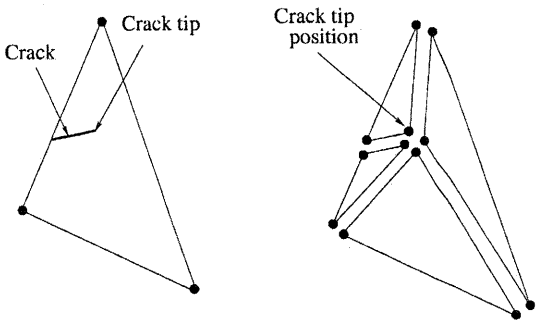


Fig. 8. Delaunay partitioning of elements containing the crack tip

domain and decreases linearly to zero on the external edge of the integral domain, see Fig. 9. This function q is explained by Combescure et al. [28], [29] . This method was originally developed in Moran and Shi [21].

To obtain the stress intensity factors K_I and K_{II} we employed the auxiliary field method [35] [25]. Two states of the cracked body are considered: the actual state, referred to as state 1, $(\sigma_{ij}^{(1)}, \epsilon_{ij}^{(1)}, u_i^{(1)})$ and an auxiliary state, state 2, $(\sigma_{ij}^{(2)}, \epsilon_{ij}^{(2)}, u_i^{(2)})$ which are the asymptotic fields for Mode I or Mode II respectively. $W^{(1,2)}$ is the strain energy in terms of the inner products $\sigma_{ij}^{(1)}\epsilon_{ij}^{(2)}$ or $\sigma_{ij}^{(2)}\epsilon_{ij}^{(1)}$.

The expression for the interaction integral is:

$$M^{(1,2)} = \int_{\mathrm{C}} \left[W^{(1,2)}\delta_{1j} - \sigma_{ij}^{(1)}\frac{\partial u_i^{(2)}}{\partial x_1} - \sigma_{ij}^{(2)}\frac{\partial u_i^{(1)}}{\partial x_1} \right] q m_j\,\mathrm{d}C \qquad (34)$$

where $C = \Gamma + C_+ + C_- + \Gamma_0$ and $\vec{m}$ is the outward unit normal to the contour C.

The interaction integral $M^{(1,2)}$ is converted into a domain integral. Using the divergence theorem and taking the limit as Γ goes to the crack tip (justified by the dominated convergence theorem, where the weighting function q would be equal to 1 at the crack tip) the interaction domain integral is:

$$M^{(1,2)} = \int_{\mathrm{A}} \left[\sigma_{ij}^{(1)}\frac{\partial u_i^{(2)}}{\partial x_1} + \sigma_{ij}^{(2)}\frac{\partial u_i^{(1)}}{\partial x_1} - W^{(1,2)}\delta_{1j} \right] \frac{\partial q}{\partial x_j}\,\mathrm{d}A \qquad (35)$$

Equation (35) assumes that the crack faces are stressfree and straight in the interior of the region A_Γ which is bounded by Γ_0 as shown in Fig. 10.

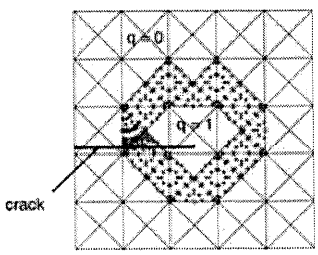


Fig. 9. Domain to compute the *J*-integral. In the dotted elements q decreases linearly to zero

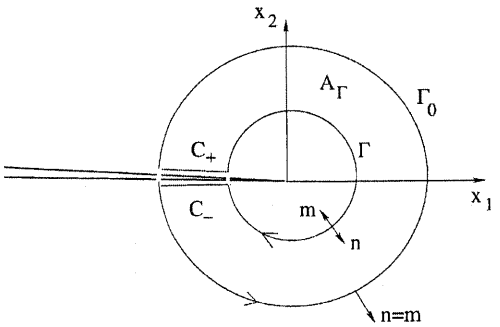


Fig. 10. Contour and domain to compute the interaction integral

Note that since Eq. (35) assumes that the crack faces are straight, the results obtained for the stress intensity factors for curved cracks are accurate only if the curvature is small (when using very fine mesh for instance). Since we assume the crack faces are straight. The results for K_2 are usually less accurate than for K_1. To improve accuracy some terms integrated along the crack faces must be added to the expression of the interaction integral.

6
Numerical examples

Several fracture mechanics problems are described to illustrate the proposed method, which we refer to as X-FEM. Recall that we use quadratic interpolants for the displacement approximation and linear interpolants for the partition of unity and the blending. Crack opening displacements, the energy error and stress intensity factors are calculated and compared with closed form and benchmark solutions. These results are also compared to an X-FEM formulation with only linear interpolants, which we will refer to as the linear X-FEM formulation.

6.1
Infinite plate

Consider an infinite plate containing a straight crack of length a and loaded by a remote uniform stress field σ. Along ABCD the closed form solution in terms of polar coordinates in a reference frame (r, θ) centered at the crack tip is:

$$\sigma_x = \frac{K_I}{\sqrt{r}}\cos\frac{\theta}{2}\left(1 - \sin\frac{\theta}{2}\sin\frac{3\theta}{2}\right) \tag{36}$$

$$\sigma_y = \frac{K_I}{\sqrt{r}}\cos\frac{\theta}{2}\left(1 + \sin\frac{\theta}{2}\sin\frac{3\theta}{2}\right) \tag{37}$$

$$\sigma_{xy} = \frac{K_I}{\sqrt{r}}\sin\frac{\theta}{2}\cos\frac{\theta}{2}\cos\frac{3\theta}{2} \tag{38}$$

The closed form near-tip displacement field is:

$$u_x = \frac{2(1+\nu)}{\sqrt{2\pi}}\frac{K_I}{E}\sqrt{r}\cos\frac{\theta}{2}\left(2 - 2\nu - \cos^2\frac{\theta}{2}\right)$$
$$u_y = \frac{2(1+\nu)}{\sqrt{2\pi}}\frac{K_I}{E}\sqrt{r}\sin\frac{\theta}{2}\left(2 - 2\nu - \cos^2\frac{\theta}{2}\right) \tag{39}$$

In the two previous expressions $K_I = \sigma\sqrt{\pi a}$ denotes the stress intensity factor, ν is Poisson's ratio and E is Young's modulus. All simulations are performed with $a = 100$ mm and $\sigma = 10^4$ N/mm^2 on a square mesh with sides of length 10 mm, as shown in Fig. 11.

On the entire boundary, displacements were prescribed by Eq. (39). The normalized energy error norm is computed by:

$$\text{energy error} = \frac{W(\varepsilon - \varepsilon^h)}{W(\varepsilon)} \tag{40}$$

where

$$W(\varepsilon) = \left(\frac{1}{2}\int_\Omega \varepsilon : \mathbf{C} : \varepsilon \, d\Omega\right)^{\frac{1}{2}} \tag{41}$$

where ε is the exact strain field and ε^h the approximate strain field obtained by the numerical solution. In Fig. 12 the error in energy is shown for the linear and the quadratic X-FEM. In Fig. 13 the convergence of the J-integral is shown. It is interesting that while the accuracy of the quadratic element is better, the rate of convergence is actually less. This behavior is probably a result of the singularity [30].

The crack opening displacement (COD) can be calculated directly from the enriched finite element approximation as follows:

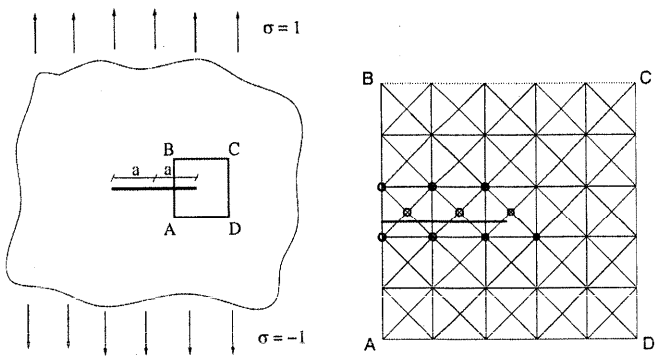


Fig. 11. Discretization around the crack tip of an infinite plate loaded by a remote stress. Nodes labeled with a circle are enriched with a step function and nodes indicated with a square are enriched with the Westergaard functions

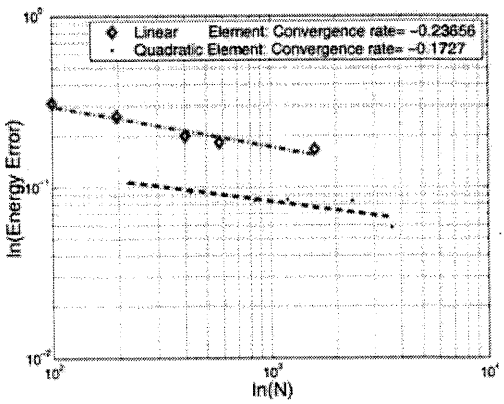


Fig. 12. Energy norm convergence for linear and quadratic formulations. N is the number of nodes

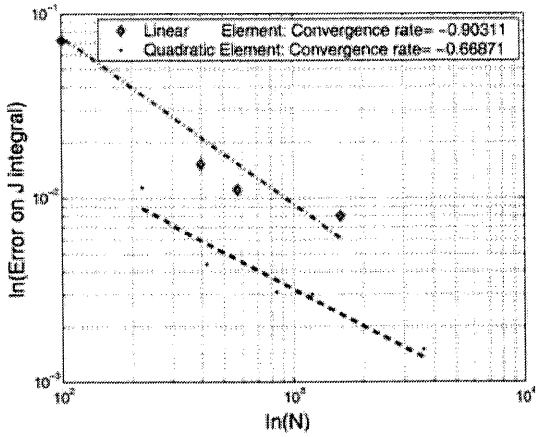


Fig. 13. J integral error as a function of number of nodes N for linear and quadratic formulations

$$[\![u^h]\!] = 2\sum_{I\in W} a_I \tilde{N}_I + 2\sqrt{r}\sum_{I\in W} b_I \tilde{N}_I \tag{42}$$

The closed form expression for the COD is:

$$[\![u]\!] = 8\sqrt{\frac{r}{2\pi}}\frac{K_I}{E}(1-\nu^2) \tag{43}$$

Figure 14 compares the COD and the horizontal component of displacement for the linear and the quadratic elements respectively. The quadratic elements provide a better match to the crack opening displacement than the linear elements. For the tangential component of the displacement jump, both the linear and quadratic element exhibit a slight anomaly at the crack tip.

6.2
Edge crack under tension

A plate is loaded by a tension $\sigma = 1.0$ psi over the top and bottom edges as shown in Fig. 15. The displacement along the y-axis is fixed at the bottom right corner, and clamped at the bottom left corner. The material parameters are 10^3 psi for Young's modulus and 0.3 for Poisson's ratio. The reference mixed mode stress intensity factors as given in [31] are:

$$K_I = \sigma\sqrt{\pi a}F\left(\frac{a}{b}\right) \tag{44}$$

where a is the crack length, b the plate width, and $F\left(\frac{a}{b}\right)$ is an empirical function. For $a/b \leq 0.6$, the function F is:

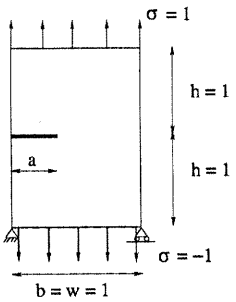


Fig. 15. Plate with edge crack under tension

$$F\left(\frac{a}{b}\right) = 1.12 - 0.231\left(\frac{a}{b}\right) + 10.55\left(\frac{a}{b}\right)^2 - 21.72\left(\frac{a}{b}\right)^3 + 30.39\left(\frac{a}{b}\right)^4 \tag{45}$$

The same type of structured mesh as shown in Fig. 16 was used except that the plate is 1×2 and the mesh is 12×12. We compared in Table 1 our results with EFG method as in [7].

For EFG, the number of cells was 10×10 and 5×5 Gauss quadrature was used in all cells except the two

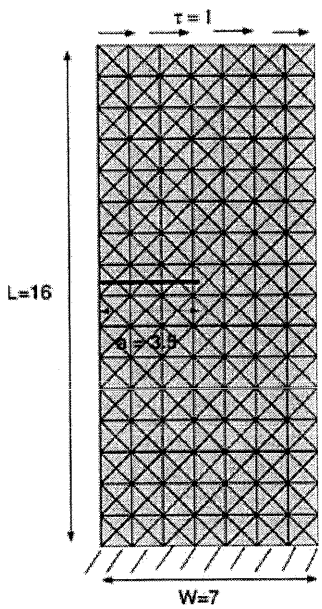


Fig. 16. Discretization of the edge crack problem under shear

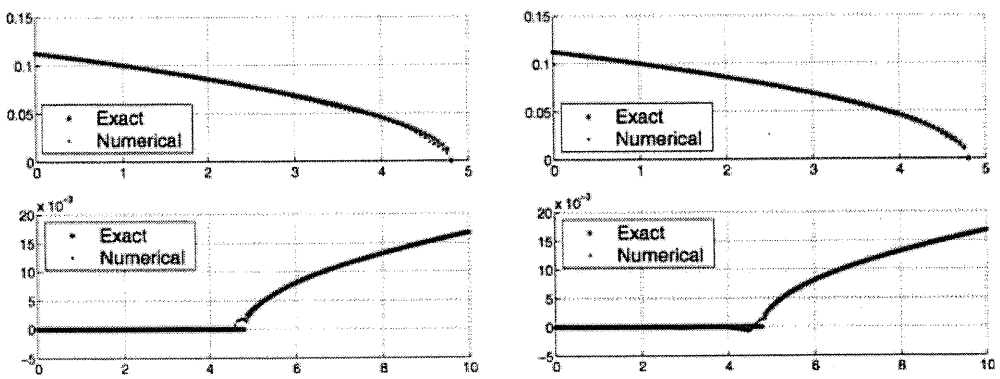


Fig. 14. Crack opening displacement (top) and tangential component of displacement along the crack (bottom) for linear (left) and quadratic (right) elements on refined mesh

Table 1. Stress intensity factors computed by quadratic XFEM compared to EFG

Crack length	K_I XFEM (linear)	K_I XFEM (quadratic)	K_I EFG by Belytschko et al. [7]	K_I exact
0.21	1.0616	1.1243	1.1401	1.1341
0.22	1.1000	1.1691	1.1779	1.1816
0.23	1.1321	1.2187	1.2487	1.2303
0.24	1.1558	1.2707	1.2807	1.2788
0.28	1.3783	1.4760	1.5036	1.4935
0.50	3.1299	3.5064	3.5512	3.5423

around the crack tip, where 9×9 Gauss quadrature was used. Quadratic XFEM seems to perform as well as the EFG method. While the EFG method tends to overestimate the stress intensity factors, quadratic XFEM tends to underestimate the result.

6.3
Edge crack under shear stress

A plate is clamped on the bottom and loaded by a shear traction $\tau = 1.0$ psi over the top edge. The material parameters are 3×10^7 psi for Young's modulus and 0.25 for Poisson's ratio. The reference mixed mode stress intensity factors as given in [35] and [31] are:

$$K_I = 34.0 \quad \text{psi}\sqrt{\text{in}}$$

$$K_{II} = 4.55 \quad \text{psi}\sqrt{\text{in}}$$

The equivalent stress intensity factor K_{eq} obtained from the J-integral for plain strain problem is:

$$J = \frac{1 - \nu^2}{E} K_{eq}^2 \tag{46}$$

The equivalent stress intensity factor is compared to $\sqrt{(K_I^2 + K_{II}^2)}$ using an elliptic criterion described in Bazant [1]. In Fig. 17, we can see that the quadratic element converges slightly faster that the linear element and is more accurate. In Fig. 18, K_I and K_{II} is seen to exhibit the same behavior.

6.4
Mixed mode crack in infinite body

The problem of an angled center crack in a body was considered as shown in Fig. 19. The plate is subjected to a far-field state of stress σ equal to unity. The crack is of length 2a and is oriented with an angle β with respect to the x-axis. The material parameters are 3×10^7 psi for Young's modulus and 0.25 for Poisson's ratio. The stress intensity factors K_I and K_{II} are given in terms of the angle β by Yau et al. [35] and Dolbow et al. [11].

$$K_I = \sigma\sqrt{(\pi a)}\cos^2(\beta) \tag{47}$$

$$K_{II} = \sigma\sqrt{(\pi a)}\sin(\beta)\cos(\beta) \tag{48}$$

where a is the half crack length. For the computations β was chosen to be 41.9872°.

Figure 20 shows the convergence for K_I and K_{II}. Good accuracy is obtained for a reasonable number of nodes. The stress intensity factors are computed by an

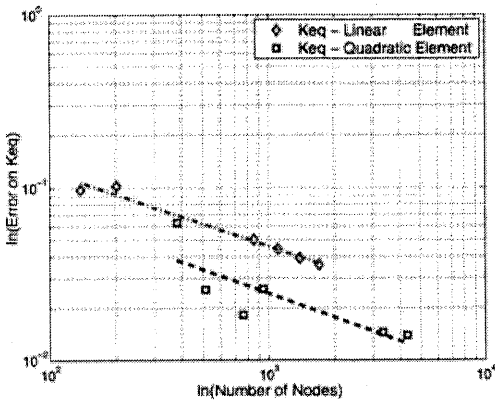


Fig. 17. Convergence for edge crack under shear. K is computed from the J-integral

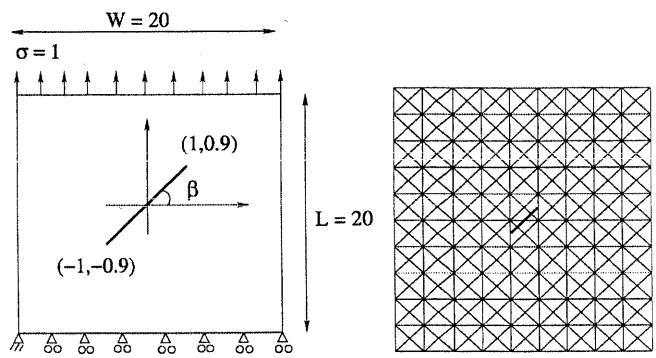
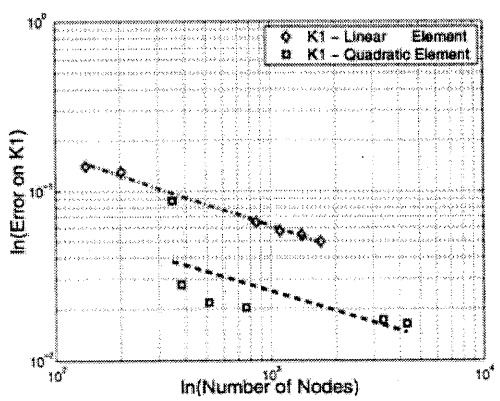


Fig. 19. Discretization used for angled crack in a plate under uniaxial tension



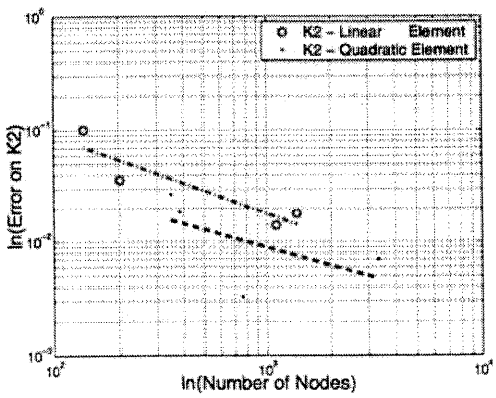


Fig. 18. Convergence for edge crack under shear. K_I and K_{II} computed by the interaction integral

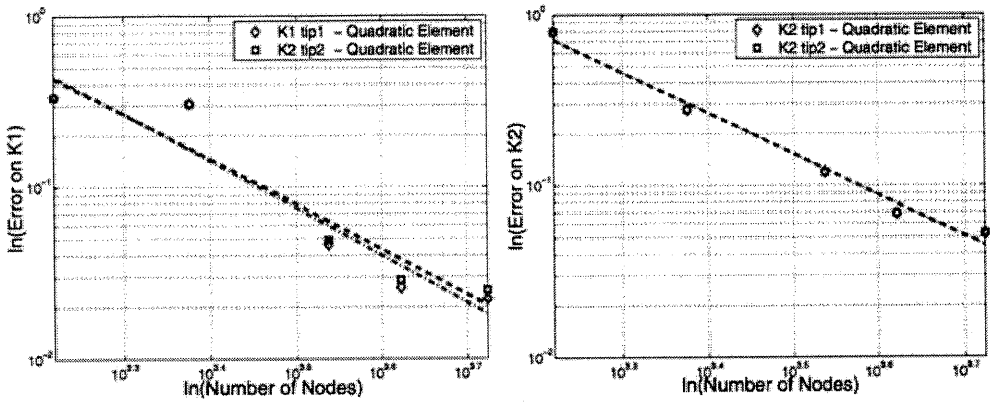


Fig. 20. Stess intensity factors error for the angled crack in infinite plate. K_I (left) and K_{II} (right) computed by the interaction integral; "tip 1" and "tip 2" refer to the two crack tips

Table 2. Stress intensity factors for angled center crack by quadratic elements

Num Nodes	$\frac{K_I}{K_I^{ana}}$ tip 1	$\frac{K_I}{K_I^{ana}}$ tip 2	$\frac{K_{II}}{K_{II}^{ana}}$ tip 1	$\frac{K_{II}}{K_{II}^{ana}}$ tip 2	Mesh
1661	0.6619	0.6647	0.2207	0.2205	11 × 21
2377	0.6916	0.6940	0.7279	0.7278	13 × 25
3449	1.0464	1.0491	1.1171	1.1172	15 × 31
4193	1.0260	1.0288	1.0670	1.0673	17 × 33
5293	1.0224	1.0251	1.0512	1.0515	19 × 37

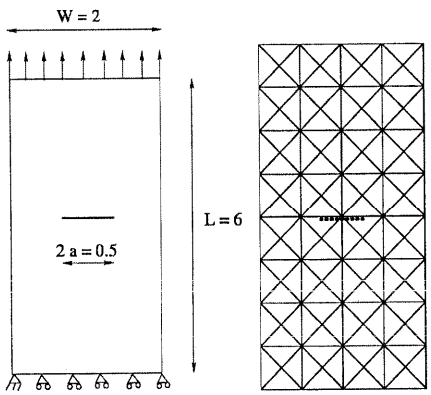


Fig. 21. Finite plate containing a centered crack

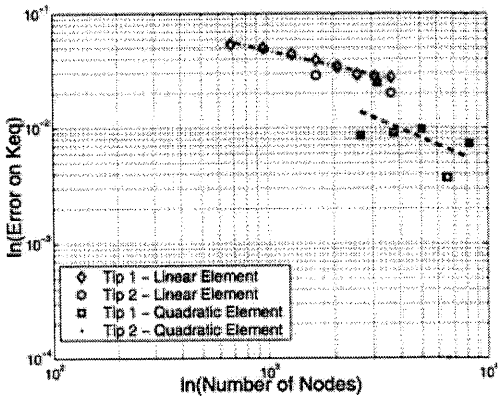


Fig. 22. Stress intensity factor error for a centered crack in a finite plate

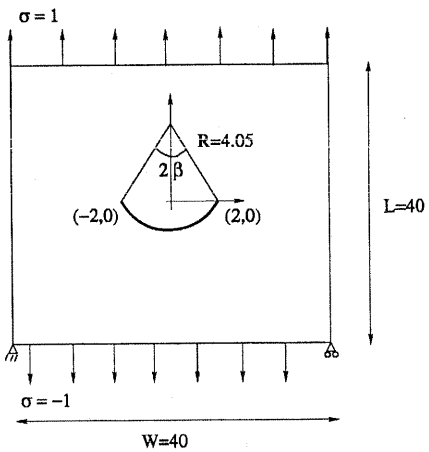


Fig. 23. Curved crack in an infinite plate

interaction integral as described in Sect. 5. For coarse discretization, the values for K_I are more accurate than the values for K_{II}. This is probably due to the fact that the computations were made in a finite body. If a larger model relative to the crack length were used this difference would have been less noticeable. The results given in Table 2 also show very good symmetry in the behavior at the two tips.

6.5 Center crack in a finite plate

The problem of a finite plate with a center crack was studied [10]. The geometry of the plate is described in Fig. 21. The analytical solution to this problem is given in Suo and Combescure [10]. The stress intensity factor is given by:

$$K_I = \sigma\sqrt{\left(\pi a \sec\left(\frac{\pi a}{2w}\right)\right)} \tag{49}$$

where a is the half crack-length and $w = W/2$ is the half width of the plate, and σ is the tensile load applied at the top of the plate.

Figure 22 shows the improved accuracy and convergence of the quadratic element over the linear element. Again, we can observe symmetric behavior at the two crack tips.

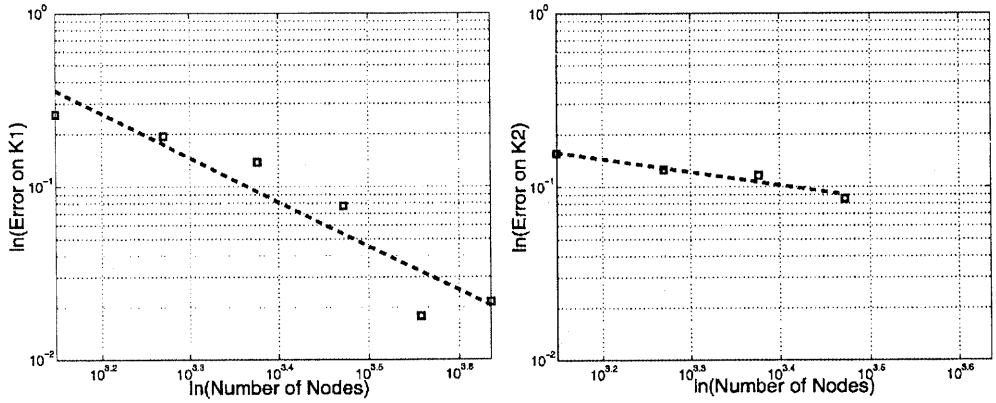


Fig. 24. Stress intensity factor error for curved crack in an infinite plate with quadratic elements. K_I (left figure) and K_{II} (right figure)

6.6 Curved crack

A curved center crack in an infinite plate is considered. A finite plate model with a large edge length to crack length ratio (> 10) was used, as shown in Fig. 23. The analytical stress intensity factors as given in Gdoutos [14] are:

$$K_I = \frac{\sigma}{2}(\pi R \sin(\beta))\left[\frac{(1-\sin^2(\beta/2)\cos^2(\beta/2))\cos(\beta/2)}{1+\sin^2(\beta/2)} + \cos(3\beta/2)\right] \quad (50)$$

$$K_{II} = \frac{\sigma}{2}(\pi R \sin(\beta))\left[\frac{(1-\sin^2(\beta/2)\cos^2(\beta/2))\sin(\beta/2)}{1+\sin^2(\beta/2)} + \sin(3\beta/2)\right] \quad (51)$$

where R is the radius of the circular arc and 2β is the subtended angle of the arc. The computations were run with $R = 4.25$ and $\beta = 28.0725°$. The stress intensity factors are $K_I = 2.0146$ and $K_{II} = 1.1116$ for the exact solution. Structured meshes were used with the following refinements: 14×14, 16×16, 18×18, 20×20, 22×22 and 24×24. The stress convergence in the intensity factor is shown in Fig. 24.

7 Conclusions

Methods for incorporating the step function and the near-field cracktip enrichment by discontinuous partitions of unity in higher order elements have been described. The implementation has been limited to a six node triangle, but it is also applicable to biquadratic quadrilaterals and higher order triangles and quadrilaterals.

The crack geometry is described by a signed distance function, and the signed distance function is also approximated by the higher order shape functions. This enables the method to treat curved cracks with more fidelity than piecewise linear approximations. We have been able to treat circular cracks and obtain more accurate results that with linear elements.

The method provides more accuracy than linear shape function elements. However, in crack problems, because of the presence of the singularity, the rate of convergence is not improved. Instead, only the absolute value of the error is improved. Furthermore, we found that it is best to use linear shape functions for the partition of unity, even when higher order functions are used for the continuous approximation.

The method is quite promising for problems where the greater accuracy of the quadratic fields is often beneficial. The method is also extensible to cohesive crack models without major modification, as in Moës and Belytschko [18].

References

1. **Bazant ZP, Planas J** (1998) Fracture and size effect in concrete and other quasibrittle materials. CRC Press, Boca Raton and London
2. **Belytschko T, Black T** (1999) Elastic crack growth in finite elements with minimal remeshing. Int. J. Numer. Meth. Eng., 45(5): 601–620
3. **Belytschko T, Moes N, Usui S, Parimi C** (2000) Arbitrary discontinuities in finite elements. Int. J. Numer. Meth. Eng., 50(4): 993–1013
4. **Belytschko T, Liu WK, Moran B** (2000) Nonlinear finite elements for continua and structures. John Wiley & Sons, Chichester
5. **Belytschko T, Gu L, Lu YY** (1994) Fracture and crack growth by element free galerkin methods. Model. Simu. Mat. Sci. Eng. 2: 519–534
6. **Belytschko T, Lu YY, Gu L** (1994) Element-free galerkin methods. Int. J. Numer. Meth. Eng. 37: 229–256
7. **Belytschko T, Lu YY, Gu L** (1995) Crack propagation by element-free galerkin methods. Eng. Frac. Mech. 51: 295–315
8. **Chen H, Belytschko T** (2003) An enriched finite element method for elastodynamic crack propagation. IJNME
9. **Chessa J, Wang HW, Belytschko T** (2003) On construction of blending elements for locally partition of unity enriched finite element methods
10. **Suo X-Z, Combescure A** (1992) Double virtual crack extension method for crack growth stability assessment. Int. J. Frac. 57: 127–150
11. **Dolbow JE, Gosz M** (2002) On the computation of mixed-mode stress intensity factors in functionally graded materials. Int. J. Soli. Struct. 39(9): 2557–2574
12. **Dolbow J, Moes N, Belytschko T** (2000) An extended finite element method for modeling crack growth with frictional contact. Comput. Meth. Appl. Mech. Eng.
13. **Fleming M, Chu YA, Moran B, Belytschko T** (1997) Enriched element-free galerkin methods for crack tip fields. Int. J. Numer. Meth. Eng. 40: 1483–1504
14. **Gdoutos E** (1993) Fracture Mechanics. Boston: Kluver Academics Publisher
15. **Gosz M, Dolbow JE, Moran B** (1998) Domain integral factor computation along curved three-dimensional interface. Int. J. Soli. Struct. 35(15): 1763–1783

16. **Gravouil A, Moes N, Belytschko T** (2001) Non-planar 3D crack growth by the extended finite element and level sets Part II: Level set update. Int. J. Numer. Meth. Eng.
17. **Melenk JM, Babuska I** (1996) The partition of unity finite element method: Basic theory and applications. Comput. Met. Appl. Mech. Eng. 39: 289–314
18. **Moes N, Belytschko T** (2002) Extended finite element method for cohesive crack growth. Eng. Frac. Mech. 69(7): 813–833
19. **Moes N, Dolbow J, Belytschko T** (1999) A finite element method for crack growth without remeshing. Int. J. Numer. Meth. Eng. 46(1): 131–150
20. **Moes N, Gravouil A, Belytschko T** (2002) Non-planar 3D crack growth by the extended finite element and level sets Part I: Mechanical model. Int. J. Numer. Meth. Eng. 53(11): 2569–2586
21. **Moran B, Shih CF** (1987) A general treatment of crack tip contour integrals. Int. J. Frac. 35: 295–310
22. **Peng D, Merriman B, Osher S, Zhao H, Kang M** (1999) A PDE-based fast local level set method. J. Comp. Phys. 155: 410–438
23. **Stolarska M, Chopp DL, Moes N, Belytschko T** (2000) Modelling crack growth by level sets and the extended finite element method. Int. J. Numer. Meth. Eng.
24. **Simo JC, Oliver J, Armero F** (1993) An analysis of strong discontinuities induced by softening solutions in rate-independent solids. J. Comput. Mech. 12: 277–296
25. **Shih C, Asaro R** (1988) Elastic-plastic analysis of cracks on bimaterial interfaces: Part 1 - small scale yielding. J. Appl. Mech. 55: 299–316
26. **Sukumar N, Moes N, Moran B, Belytschko T** (2000) Extended finite element method for three-dimensional crack modeling. Int. J. Numer. Meth. Eng. 48(11): 1549–1570
27. **Sukumar N, Chopp DL, Moës N, Belytschko T** (2001) Modeling holes and inclusions by level sets in the extended finite element method. Comput. Meth. Appl. Mech. Eng. 90(46,47): 6183–6200
28. **Suo XZ, Combescure A** (1989) Sur une formulation mathématique de la dérivée seconde de l'énergie potentielle en théorie de la rupture fragile. Compte-Rendu de l'Académie des Sciences de Paris, t. 308(II): 1119–1122
29. **Suo XZ, Valeta MP** (1998) Second variation of energy and an associated line independent integral in fracture mechanics. II Numerical validations. Eur. J. Mech. A/Solids 17(4): 541–565
30. **Szabo BA, Babuska I** (1991) Finite Element Analysis. New York, Wiley
31. **Tada H, Paris PC, Irwin R** (1973) The stress analysis of cracks, Handbook. Del Research Corporation, Hellertown, Pennsylvania
32. **Ventura G, Xu JX, Belytschko T** (2002) A vector level set method and new discontinuity approximations for crack growth by EFG. Int. J. Numer. Meth. Eng. 54:
33. **Ventura G, Xu JX, Belytschko T** (2002) Level set crack propagation modelling in the element free Galerkin methods. Proceedings ECCM-2001, European conference on Computation Mechanics, Krakow, 26–29 June 2001
34. **Wells GN, Sluys LJ, de Borst R** (2002) Simulating the propagation of displacement discontinuities in a regularized strain-softening medium. Int. J. Numer. Meth. Eng. 53(5): 1235–1256
35. **Yau JF, Wang SS, Corten HT** (1980) A mixed-mode crack analysis of isotropic solids using conversation laws of elasticity. J. Appl. Mech. 47: 335–341